



ELSEVIER

Contents lists available at ScienceDirect

Computers and Structures

journal homepage: www.elsevier.com/locate/compstruc

Non-parametric shape optimization method for natural vibration design of stiffened shells

Yang Liu ^{a,*}, Masatoshi Shimoda ^b^a*Department of Mechanical Engineering, Osaka University, 2-1, Yamadaoka, Suita, Osaka 567-0047, Japan*^b*Department of Advanced Science and Technology, Toyota Technological Institute, 2-12-1 Hisakata, Tempaku-ku, Nagoya 468-8511, Japan*

ARTICLE INFO

Article history:

Received 8 February 2014

Accepted 21 August 2014

Available online 1 October 2014

Keywords:

Natural vibration
Eigenvalue maximization
Volume minimization
Shape optimization
Non-parametric
Stiffened shells

ABSTRACT

In this paper, we newly present an effective shape optimization method for natural vibration design of stiffened thin-walled or shell structures. Both the stiffeners and their basic structures are optimized by solving two kinds of optimization problems. The first is a specified eigenvalue maximization problem subject to a volume constraint, and the second is its reciprocal volume minimization problem subject to a specified eigenvalue constraint. The boundary shapes of a thin-walled structure are determined under the condition where the stiffeners and the basic structure are movable in the in-plane direction to their surface. Both problems are formulated as distributed-parameter shape optimization problems, and the shape gradient functions are derived using the material derivative method and the adjoint variable method. The optimal free-boundary shapes are determined by applying the derived shape gradient function to the H^1 gradient method for shells, which is a parameter-free shape optimization method proposed by one of the authors. Several design examples are presented to validate the proposed method and demonstrate its practical usages.

© 2014 Elsevier Ltd. All rights reserved.

1. Introduction

Thin-walled or shell structures are widely used as basic structural components in various industrial products such as car bodies, aircraft fuselages, pressure vessels as well as in bridges and buildings. They are commonly stiffened by stiffeners to improve the bending rigidity of the basic structures. With recent enhancements of high speed, high function and substantial weight reduction of thin-walled structures, the vibration design in consideration of the dynamic characteristics has become more important than ever. The natural frequencies (i.e., vibration eigenvalues) usually represent the dynamic characteristics of structures, especially the lower order natural frequencies are considered as an evaluation measure of the dynamic stability. The dynamic response of structures can be reduced by increasing their lower order natural frequencies [1,2]. Moreover, the reduction of the dynamic response of a structure generally leads to the minimum weight for the structure design [3].

In terms of the optimum design of stiffened thin-walled structures under either static or dynamic loading conditions, investigations have been extensively carried out to achieve better static or dynamic performance as well as a lighter weight. Most of the

investigations focused on determining the best layout configurations for stiffeners on thin-walled structures. For example, Cheng and Olhoff [4] reported a method of generating the optimal stiffener layout pattern for maximizing the integral stiffness of a solid elastic plate by using the plate thickness function as the design variable. Luo and Gea [5,6] used a systematic topology optimization based approach to design the optimal location and orientation of stiffeners for static and interior sound reduction problems. Liu et al. [7] studied the eigenvalue sensitivity with respect to the location of stiffeners for a stiffened plate. Ding and Yamazaki [8] introduced a growing and branch tree model to generate stiffener layout patterns on plate structures for vibration design problems. Bojczuk and Szteleblak [9] showed an application of a method based on sensitivity analysis combined with an adjoint method to the optimization of 2D structures with respect to the deployment of stiffeners. Many investigations have also dealt with size design optimization of stiffener geometrical properties, such as their number [10,11], thickness [12], cross-section dimensions [13,14], and spacing [15]. On the other hand, few studies contribute to the shape optimization of the stiffeners and their basic structure, though the optimum shape design can greatly influence the static and dynamic characteristics as well as weight [16,17]. As one of the few studies, the authors recently developed a parameter-free shape optimization method to deal with the shape optimum design of stiffeners on thin-walled structures [18]. In this

* Corresponding author. Tel.: +81 6 68794121; fax: +81 6 68794121.

E-mail addresses: liuyang60212@gmail.com, ryu@comec.mech.eng.osaka-u.ac.jp (Y. Liu), shimoda@toyota-ti.ac.jp (M. Shimoda).

method, we employed the adjoint variable method and the shape updating approach by traction force to solve difficulties of the large-scale design variables problem and the jagged boundary problem [19] in the parameter-free shape optimization. Bletzinger [20] proposed the sensitivity filtering technique to solve these difficulties in their parameter-free method. To the best of our knowledge, no other group has applied the parameter-free method to the stiffener design problem. However, only the compliance minimization problem was solved simply as a self-adjoint problem in our previous work [18], in which the basic structure was assumed not to be varied. It is not available for the vibration design in consideration of the dynamic characteristics, which is known as a more complicated design problem.

For the natural vibration problem of stiffened shells, this paper newly presents a parameter-free shape optimization of both the stiffeners and their basic structures on stiffened shells. Two kinds of natural vibration design problems are treated as parameter-free shape optimization problems. One is a specified eigenvalue maximization problem subject to a volume constraint, and the other is its reciprocal volume minimization problem subject to a specified eigenvalue constraint. We formulate the two design problems in the continuous system, or in the function space, which enables our method to create the optimal shapes without any shape parameterization and discretization in advance. In other words, the shape obtained is not influenced by the parameterization and the discretization. Sensitivity functions (i.e., shape gradient functions) for both stiffeners and the basic structure are theoretically derived using the material derivative method and the adjoint variable method. The direct derivatives of the element stiffness matrix are not required in the sensitivity calculation. Therefore, it can be easily implemented in combination with a commercial FEM code and the shape optimization of practical shell structures is easily computable even if it is complicated. After that, the negative shape gradient function derived is applied as a distributed force to free boundaries of the stiffeners and the basic structure to vary the shapes. This approach makes it possible both to reduce the objective functional and to maintain the mesh regularization simultaneously. Moreover, the target vibration mode is considered as the one receiving the most attention or being disadvantageous in the practical design. To eliminate difficulties caused by repeated eigenvalues, i.e., mode switching or frequency crossing during optimization [21], the Modal Assurance Criterion (MAC) [22] is adopted to track the specified natural mode through changes in the eigenvalue maximization or eigenvalue constraint problem.

In the following section, the governing equation of the natural vibration of a shell will be described. Next, the formulation of design problems and the derivation of each shape gradient function will be presented in Section 3. After explaining the details of the optimization method in Section 4, the validity and practical utility of this method will be verified through several design examples in Section 5.

2. Variational equation for natural vibration of shell modeled by infinitesimal flat plates

As shown in Fig. 1 and Eqs. (1)–(3) basic shell structure or stiffener with an initial bounded domain $\Omega \subset \mathbb{R}^3$ is defined by the mid-area A and the domain of thickness direction $(-h/2, h/2)$, and the side surface S is defined by the boundary ∂A of the mid-area A .

$$\Omega = \{(x_1, x_2, x_3) \in \mathbb{R}^3 | (x_1, x_2) \in A \subset \mathbb{R}^2, x_3 \in (-h/2, h/2)\}, \quad (1)$$

$$\Omega = A \times (-h/2, h/2), \quad (2)$$

$$S = \partial A \times (-h/2, h/2). \quad (3)$$

In the structural analysis of a shell with arbitrary geometry, a practical approach is to model the shell by a set of infinitesimal flat plates, that is not only for simplicity but also frequently performs

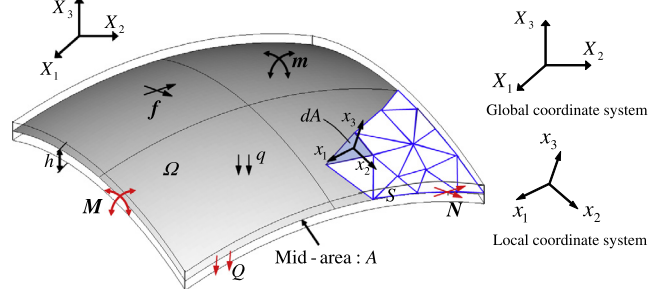


Fig. 1. Shell geometry assembled by infinitesimal flat plates.

quite well in curved shell applications [23]. As shown in Fig. 1, each flat plate dA has a local coordinate system (i.e., plate coordinate system) that is fixed with respect to its geometry and independent of the unique coordinate system used at all points on the shell (i.e., global coordinate system). Both coordinate systems are constructed as a Cartesian coordinate system. The transformation between degrees of freedom in the local coordinates, u^l , and in the global coordinate, u^g , is calculated in Eq. (4).

$$u_j^l = T_{ij}^{gl} u_i^g, \quad (4)$$

where T^{gl} indicates the global-local transformation tensor. The displacement expressed by the local coordinates $u^l = \{u_i^l\}_{i=1,2,3}$ is considered by dividing it into the displacement in the in-plane direction u_x and the displacement in the out-of-plane direction u_3^l . In this paper, the subscripts of the Greek letters are expressed as $\alpha, \beta, \gamma, \delta = 1, 2$, the tensor subscript notation uses Einstein's summation convention and a partial differential notation for the spatial coordinates $(\cdot)_{,i} = \partial(\cdot)/\partial x_i$.

The Mindlin-Reissner plate theory is applied for each flat plate dA and a plate bending stiffness and membrane stiffness are combined in its local coordinate system [24]. In the local coordinate system of dA shown in Fig. 2, the membrane action is expressed by the in-plane displacement u_{0x} of the mid-area, and the bending action is expressed by the out-of-plane displacement w , and the rotational angle θ_x . The Mindlin-Reissner plate theory posits the following conditions with respect to the displacement of a general point on dA in its local coordinate system.

$$u_x^l(x_1, x_2, x_3) \equiv u_{0x}(x_1, x_2) - x_3 \theta_x(x_1, x_2), \quad (5)$$

$$u_3^l(x_1, x_2, x_3) \equiv w(x_1, x_2), \quad (6)$$

When assembling the flat plates to model the curved shell, the bending and membrane stiffness are coupled only on the interelement boundaries due to differences between adjacent plate orientations. Since the shell dealt with in our manuscript is assumed to be assembled by infinitesimal flats, the differences should be extremely small and the coupling effects can be neglected. Moreover, it should be remarked that the formulation of a shell modeled as an assembly of flat plates requires the handling of different coordinate systems, and the bending stiffness and the membrane stiffness as well as the force vector should be transformed from local coordinates to the global coordinate. However, for the sake of brevity, this

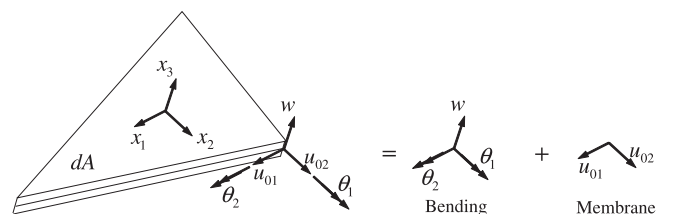


Fig. 2. Formulation of an infinitesimal flat plate dA in its local coordinate system.

issue is not treated here in detail. For further information on the formulation see the reference [24].

Then, the weak formed eigenvalue equation for natural vibration in terms of r th mode $(u_0^{(r)}, w^{(r)}, \theta^{(r)}) \in U$ can be expressed as Eq. (7) by substituting Eqs. (5) and (6) into the variational equation (i.e., weak form) of the three-dimensional linear elastic eigenvalue theory, eliminating ε_{33} .

$$\begin{aligned} a((u_0^{(r)}, w^{(r)}, \theta^{(r)}), (\bar{u}_0, \bar{w}, \bar{\theta})) &= \lambda^{(r)} b((u_0^{(r)}, w^{(r)}, \theta^{(r)}), \\ (\bar{u}_0, \bar{w}, \bar{\theta})), (u_0^{(r)}, w^{(r)}, \theta^{(r)}) \in U, \forall (\bar{u}_0, \bar{w}, \bar{\theta}) \in U, \end{aligned} \quad (7)$$

where (\cdot) expresses a variation and U expresses the admissible space in which the given constraint conditions of (u_0, w, θ) is satisfied. $\lambda^{(r)}$ indicates the eigenvalue of the r th natural mode. In addition, the bilinear forms $a(\cdot, \cdot)$ and $b(\cdot, \cdot)$ are defined respectively as shown below.

$$\begin{aligned} a((u_0^{(r)}, w^{(r)}, \theta^{(r)}), (\bar{u}_0, \bar{w}, \bar{\theta})) &= \int_{\Omega} \{C_{\alpha\beta\gamma\delta}(u_{0\alpha,\beta} - x_3\theta_{\alpha,\beta})(\bar{u}_{0\gamma,\delta} - x_3\bar{\theta}_{\gamma,\delta}) \\ + C_{\alpha\beta\gamma\delta}^S u_{0\gamma,\delta}\} d\Omega = \int_A \{c_{\alpha\beta\gamma\delta}^B \theta_{(\gamma,\delta)}^r \bar{\theta}_{(\alpha,\beta)} + c_{\alpha\beta\gamma\delta}^M u_{0\gamma,\delta}^{(r)} \bar{u}_{0\alpha,\beta} + k c_{\alpha\beta\gamma\delta}^S \gamma_{\alpha}^{(r)} \bar{\gamma}_{\beta}\} dA, \end{aligned} \quad (8)$$

$$b((u_0^{(r)}, w^{(r)}, \theta^{(r)}), (\bar{u}_0, \bar{w}, \bar{\theta})) = \rho \int_A \{h(w^{(r)}\bar{w} + u_{0x}^{(r)}\bar{u}_{0x}) + I\theta_x^{(r)}\bar{\theta}_x\} dA, \quad (9)$$

where $\{C_{\alpha\beta\gamma\delta}\}_{\alpha,\beta,\gamma,\delta=1,2}$ and $\{c_{\alpha\beta}^S\}_{\alpha,\beta=1,2}$ express an elastic tensor with respect to the membrane stress and the shearing stress, respectively. $c_{\alpha\beta\gamma\delta}^B$, $c_{\alpha\beta}^S$ and $c_{\alpha\beta\gamma\delta}^M$ express an elastic tensor with respect to bending, shearing and membrane components, respectively, when considering through-thickness integration by the iterated integral $\int_{\Omega}(\cdot)d\Omega = \int_A \int_{-h/2}^{h/2}(\cdot)dz dA$. $\theta_{(\alpha,\beta)} (= \frac{1}{2}(\theta_{\alpha,\beta} + \theta_{\beta,\alpha}))$ expresses the curvatures and $\gamma_x (= w_{,x} - \theta_{,x})$ expresses the transverse shear strains. Moreover, ρ and $I (= h^3/12)$ express a mass density and a second moment of area, respectively. The constant k denotes a shear correction factor, which can be used as $k = 5/6$ within Reissner theory of isotropic elastic plates [25].

3. Shape optimization problem of stiffened shells

3.1. Domain variation

A stiffened shell structure consists of a basic shell structure $\{\Omega^i\}_{i=0}$ and stiffeners $\{\Omega^i_s\}_{i=1,2,\dots,N}$, where N is the number of stiffeners. To determine the optimal free-boundary shapes of the basic structure or stiffeners, the shape variations are considered as in-plane variations \mathbf{V}^i in the tangential direction to the surfaces. In response to the practical design problems, the basic structure and stiffeners varied separately or simultaneously.

As shown in Fig. 3, consider that a linear elastic basic structure or stiffeners having an initial domain Ω^i , mid-area A^i , boundary ∂A^i and side surface S^i undergoes domain variation \mathbf{V}^i (i.e., design velocity field) in the in-plane direction such that its domain, mid-area, boundary and side surface become Ω_s^i , A_s^i , ∂A_s^i , and S_s^i , respectively. It is assumed that the plate thickness h remains constant with respect to the domain variation. The domain variation at this time can be expressed by a mapping from A^i to A_s^i , which is denoted as $T_s : X \in A \mapsto X_s(X) \in A_s^i$, $0 \leq s \leq \varepsilon$ (ε is a small integer) given by $X_s = T_s(X)$, $A_s^i = T_s(A^i)$ [26,27]. The subscript s expresses the iteration history of the domain variation. Assuming a shape constraint is acting on the variation in the domain, the infinitesimal variation of the domain can be expressed by

$$T_{s+\Delta s}(X) = T_s(X) + \Delta s \mathbf{V}^i, \quad (10)$$

where the design velocity field $\mathbf{V}^i(X_s^i) = \partial T_s(X)/\partial s$. The non-parametric shape optimization method explained later is a method for determining the optimal domain variation \mathbf{V}^i .

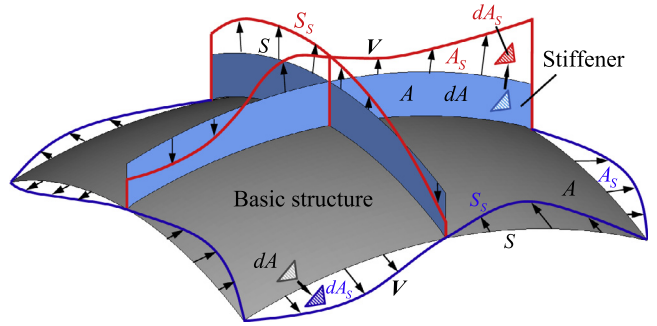


Fig. 3. Shape variation of stiffeners and the basic shell by \mathbf{V}^i .

3.2. Eigenvalue maximization problem

Letting the eigenvalue equation in Eq. (7) and the volume be the constraint conditions and the eigenvalue of the specified r th natural mode be the objective functional to be maximized, a distributed-parameter shape optimization problem for finding the optimal design velocity field of the stiffeners \mathbf{V}^i , or $A_s^i (= A^i + \Delta s \mathbf{V}^i)$ can be formulated as shown below:

$$\text{Given } \{A^i\}_{i=0,1,2,\dots,N}, \quad (11)$$

$$\text{find } \{\mathbf{V}^i\}_{i=0,1,2,\dots,N} \text{ (or } \{A_s^i\}_{i=0,1,2,\dots,N}), \quad (12)$$

$$\text{that minimizes } -\lambda^{(r)}, \quad (13)$$

$$\text{subject to Eq. (7) and} \quad (14)$$

$$M = \sum_{i=0}^{N^*} M^i \left(= \int_{A^i} h^i dA \right) \leq \hat{M}, \quad (15)$$

where M and \hat{M} denote the volume of the thin-walled structure with ($N^* = N$) or without ($N^* = 0$) stiffeners and its constraint value, respectively.

For the repeated eigenvalue problems as mentioned in Section 1, the Modal Assurance Criterion (MAC) [22] defined in Eq. (16) is used to track the specified r th natural mode of the initial shape. The mode with a maximum value of MAC in all natural modes is regarded as the corresponding mode and is tracked.

$$\text{MAC}(\phi_0^{(r)}, \phi_s) = \frac{|\{\phi_0^{(r)}\}^T \{\phi_s\}|^2}{\left(\{\phi_0^{(r)}\}^T \{\phi_0^{(r)}\}\right) \left(\{\phi_s\}^T \{\phi_s\}\right)}, \quad (16)$$

$$\phi_s^{(r)*} = \left\{ \left(u_0^{(r)*}, w^{(r)*}, \theta^{(r)*} \right) | \text{MAC}(\phi_0^{(r)}, \phi_s^{(r)*}) \text{ is the maximum value} \right\}, \quad (17)$$

where $\phi_0^{(r)}$ and ϕ_s indicate the eigenvectors of the r th mode of the initial shape and each mode of the varied shape, respectively. The MAC is normalized by the magnitude of the eigenvectors and, thus, is a real-valued scalar taking on values from 0 to 1. $\text{MAC} = 0$ represents no consistent correspondence and $\text{MAC} = 1$ represents a consistent correspondence. $\phi_s^{(r)*}$ in Eq. (17) denotes the corresponding mode with a maximum value of MAC. Then, the tracked eigenvectors $(u_0^{(r)*}, w^{(r)*}, \theta^{(r)*})$ are used to calculate the sensitivity function of the eigenvalue maximization problem as well as the volume minimization problem in Section 3.3.

The shape design sensitivity analysis in this paper is based on the material derivative idea of continuum mechanics and the adjoint variable method, which were particularly introduced by Haug et al. [26] and Choi and Kim [27]. When the objective functional J is given as a domain integral of the distributed function Ψ_s ,

$$J = \int_{\Omega_s} \Psi_s d\Omega, \quad (18)$$

the material derivative j is given by

$$J = \int_{\Omega} \Psi' d\Omega + \int_{\Gamma} \Psi V_n d\Gamma, \quad (19)$$

where $V_n = n_i V_i$, the vector n is an outward normal unit vector to the boundary and $(\cdot)'$ indicates a shape derivative (Lagrange derivative).

When the objective functional J is given as a boundary integral of the distributed function Ψ_s ,

$$J = \int_{\Gamma_s} \Psi_s d\Gamma, \quad (20)$$

the material derivative \dot{J} is given by

$$\dot{J} = \int_{\Gamma} \{\Psi' + (\Psi_i n_i + \Psi H) V_n\} d\Gamma, \quad (21)$$

where H expresses twice the mean curvature of Γ in \mathbb{R}^3 .

Letting $(\bar{u}_0, \bar{w}, \bar{\theta})$ and Λ_M denote the Lagrange multipliers for the eigenvalue equation and volume constraints, respectively, the Lagrange functional L associated with this problem can be expressed as

$$\begin{aligned} L(A^i, (u_0^{(r)*}, w^{(r)*}, \theta^{(r)*}), (\bar{u}_0, \bar{w}, \bar{\theta}), \Lambda_M) \\ = -\lambda^{(r)} + \lambda^{(r)} b((u_0^{(r)*}, w^{(r)*}, \theta^{(r)*}), (\bar{u}_0, \bar{w}, \bar{\theta})) \\ - a((u_0^{(r)*}, w^{(r)*}, \theta^{(r)*}), (\bar{u}_0, \bar{w}, \bar{\theta})) + \Lambda_M(M - \hat{M}). \end{aligned} \quad (22)$$

Then, the material derivative \dot{L} of the Lagrange functional can be derived as shown in Eq. (23) using Eqs. (18)–(21) [26,27].

$$\begin{aligned} \dot{L} = -a((u_0^{(r)*}, w^{(r)*}, \theta^{(r)*}), (\bar{u}_0, \bar{w}, \bar{\theta})) + \lambda^{(r)} b((u_0^{(r)*}, w^{(r)*}, \theta^{(r)*}), \\ (\bar{u}_0, \bar{w}, \bar{\theta})) - a((u_0^{(r)*}, w^{(r)*}, \theta^{(r)*}), (\bar{u}'_0, \bar{w}', \bar{\theta}')) \\ + \lambda^{(r)} b((u_0^{(r)*}, w^{(r)*}, \theta^{(r)*}), (\bar{u}'_0, \bar{w}', \bar{\theta}')) + \lambda^{(r)} \{b((u_0^{(r)*}, w^{(r)*}, \theta^{(r)*}), \\ (\bar{u}_0, \bar{w}, \bar{\theta})) - 1\} + \dot{\Lambda}_M(M - \hat{M}) + \langle G_{\partial A^i} n_{\partial A^i}, \mathbf{V}^i \rangle_{\partial A^i}, \quad \mathbf{V}^i \in C_{\Theta}. \end{aligned} \quad (23)$$

where

$$\begin{aligned} \langle G_{\partial A^i} n_{\partial A^i}, \mathbf{V}^i \rangle_{\partial A^i} &\equiv \sum_{i=0}^N \int_{\partial A^i} G_{\partial A^i} n_{\partial A^i} \cdot \mathbf{V}^i dS \\ &= \sum_{i=0}^N \int_{\partial A^i} \left[-c_{\alpha\beta\gamma\delta}^B \theta_{(\alpha,\beta)}^{(r)*} \bar{\theta}_{(\gamma,\delta)} - k c_{\alpha\beta}^S (\theta_{\beta}^{(r)*} - w_{\beta}^{(r)*}) (\bar{\theta}_{\alpha} - \bar{w}_{\alpha}) \right. \\ &\quad \left. - c_{\alpha\beta\gamma\delta}^M u_{0\alpha\beta}^{(r)*} \bar{u}_{0\gamma\delta} + \lambda^{(r)} \rho \{h(w^{(r)*} \bar{w} + u_{0\alpha}^{(r)*} \bar{u}_{0\alpha}) \right. \\ &\quad \left. + I \theta_{\alpha}^{(r)*} \bar{\theta}_{\alpha}\} + \Lambda_M \right] n_{\partial A^i} \cdot \mathbf{V}^i dS, \end{aligned} \quad (24)$$

The notation $n_{\partial A^i}$ in Eq. (24) is defined as an in-plane outward unit normal vector on boundary ∂A^i . Additionally, C_{Θ} expresses the admissible function space that satisfies the constraints of domain variation. The notation $(\cdot)'$ and (\cdot) are the shape derivative and the material derivative with respect to the domain variation, respectively [26,27].

The optimality conditions of the Lagrangian function L with respect to $(\bar{u}_0^{(r)*}, \bar{w}^{(r)*}, \bar{\theta}^{(r)*})$ and Λ_M are expressed as shown below.

$$a((u_0^{(r)*}, w^{(r)*}, \theta^{(r)*}), (\bar{u}'_0, \bar{w}', \bar{\theta}')) = \lambda^{(r)} b((u_0^{(r)*}, w^{(r)*}, \theta^{(r)*}), \\ (\bar{u}'_0, \bar{w}', \bar{\theta}')), \forall (\bar{u}'_0, \bar{w}', \bar{\theta}') \in U, \quad (25)$$

$$a((u_0^{(r)*}, w^{(r)*}, \theta^{(r)*}), (\bar{u}_0, \bar{w}, \bar{\theta})) = \lambda^{(r)} b((u_0^{(r)*}, w^{(r)*}, \theta^{(r)*}), \\ (\bar{u}_0, \bar{w}, \bar{\theta})), \forall (u^{(r)*}, w^{(r)*}, \theta^{(r)*}) \in U, \quad (26)$$

$$b((u_0^{(r)*}, w^{(r)*}, \theta^{(r)*}), (\bar{u}_0, \bar{w}, \bar{\theta})) = 1, \quad (27)$$

$$\dot{\Lambda}_M(M - \hat{M}) = 0, \quad (28)$$

$$\Lambda_M \geq 0, \quad (29)$$

$$M - \hat{M} \leq 0. \quad (30)$$

When the optimality conditions with respect to the state variable $(u_0^{(r)*}, w^{(r)*}, \theta^{(r)*})$, the adjoint variable $(\bar{u}_0, \bar{w}, \bar{\theta})$ and Λ_M are satisfied, Eq. (23) becomes

$$\dot{L} = \langle G_{\partial A^i} n_{\partial A^i}, \mathbf{V}^i \rangle_{\partial A^i}, \mathbf{V}^i \in C_{\Theta}. \quad (31)$$

The sensitivity function (i.e., the shape gradient function) for this problem is derived as Eq. (32) by considering the relationship as shown in (33).

$$\begin{aligned} G_{\partial A^i} = -c_{\alpha\beta\gamma\delta}^B \theta_{(\alpha,\beta)}^{(r)*} \bar{\theta}_{(\gamma,\delta)} - k c_{\alpha\beta}^S (\theta_{\beta}^{(r)*} - w_{\beta}^{(r)*}) (\bar{\theta}_{\alpha} - \bar{w}_{\alpha}) - c_{\alpha\beta\gamma\delta}^M u_{0\alpha\beta}^{(r)*} \bar{u}_{0\gamma\delta} \\ + \lambda^{(r)} \rho \{h(w^{(r)*} \bar{w} + u_{0\alpha}^{(r)*} \bar{u}_{0\alpha}) + I \theta_{\alpha}^{(r)*} \bar{\theta}_{\alpha}\} + \Lambda_M. \end{aligned} \quad (32)$$

$$(\bar{u}_0, \bar{w}, \bar{\theta}) = \frac{(u_0^{(r)*}, w^{(r)*}, \theta^{(r)*})}{b((u_0^{(r)*}, w^{(r)*}, \theta^{(r)*}), (u_0^{(r)*}, w^{(r)*}, \theta^{(r)*}))} \quad (33)$$

3.3. Volume minimization problem

With the aim of designing the lightweight of stiffened thin-walled structures, we formulate the reciprocal problem of that treated in the preceding section. Letting the eigenvalue equation in Eq. (7) and the eigenvalue of the specified r th natural mode be the constraint conditions and the volume be the objective functional to be minimized. A distributed-parameter shape optimization problem is expressed as shown below:

$$\text{Given } \{A^i\}_{i=0,1,2,\dots,N}, \quad (34)$$

$$\text{find } \{\mathbf{V}^i\}_{i=0,1,2,\dots,N} \left(\text{or } \{A_s^i\}_{i=0,1,2,\dots,N} \right), \quad (35)$$

$$\text{that minimizes } M = \sum_{i=0}^N M^i \left(= \int_{A^i} h dA \right), \quad (36)$$

$$\text{subject to Eq. (7) and} \quad (37)$$

$$\lambda^{(r)} = \hat{\lambda}^{(r)}, \quad (38)$$

where $\hat{\lambda}^{(r)}$ is the constraint value of the eigenvalue of the specified r th natural mode.

Letting $(\bar{u}_0, \bar{w}, \bar{\theta})$ and Λ_{λ} denote the Lagrange multipliers for the state equation and eigenvalue constraints, respectively, the Lagrange functional L associated with this problem can be expressed as

$$\begin{aligned} L(A^i, (u_0^{(r)*}, w^{(r)*}, \theta^{(r)*}), (\bar{u}_0, \bar{w}, \bar{\theta}), \Lambda) \\ = M + \lambda^{(r)} b((u_0^{(r)*}, w^{(r)*}, \theta^{(r)*}), (\bar{u}_0, \bar{w}, \bar{\theta})) \\ - a((u_0^{(r)*}, w^{(r)*}, \theta^{(r)*}), (\bar{u}'_0, \bar{w}', \bar{\theta}')) + \Lambda_{\lambda} (\lambda^{(r)} - \hat{\lambda}^{(r)}). \end{aligned} \quad (39)$$

Using the design velocity field \mathbf{V}^i to indicate the amount of domain variation of the basic structure or stiffeners, the material derivative \dot{L} of the Lagrangian functional L can be expressed as

$$\begin{aligned} \dot{L} = -a((u_0^{(r)*}, w^{(r)*}, \theta^{(r)*}), (\bar{u}_0, \bar{w}, \bar{\theta})) \\ + \lambda^{(r)} b((u_0^{(r)*}, w^{(r)*}, \theta^{(r)*}), (\bar{u}_0, \bar{w}, \bar{\theta})) \\ - a((u_0^{(r)*}, w^{(r)*}, \theta^{(r)*}), (\bar{u}'_0, \bar{w}', \bar{\theta}')) \\ + \lambda^{(r)} b((u_0^{(r)*}, w^{(r)*}, \theta^{(r)*}), (\bar{u}'_0, \bar{w}', \bar{\theta}')) \\ + \dot{\lambda}^{(r)} \{b((u_0^{(r)*}, w^{(r)*}, \theta^{(r)*}), (\bar{u}_0, \bar{w}, \bar{\theta})) - \Lambda_{\lambda}\} \\ + \dot{\Lambda}_{\lambda} (\lambda^{(r)} - \hat{\lambda}^{(r)}) + \langle G_{\partial A^i} n_{\partial A^i}, \mathbf{V}^i \rangle_{\partial A^i}, \mathbf{V}^i \in C_{\Theta}, \end{aligned} \quad (40)$$

where

$$\begin{aligned} \left\langle G_{\partial A^i} n_{\partial A^i}, \mathbf{V}^i \right\rangle_{\partial A^i} &\equiv \sum_{i=0}^N \int_{\partial A^i} G_{\partial A^i} n_{\partial A^i} \cdot \mathbf{V}^i dS \\ &= \sum_{i=0}^N \int_{\partial A^i} \left[1 - A_\lambda \left\{ -c_{\alpha\beta\gamma\delta}^B \theta_{(\alpha,\beta)}^{(r)*} \bar{\theta}_{(\gamma,\delta)} - k c_{\alpha\beta}^S \left(\theta_\beta^{(r)*} - w_{,\beta}^{(r)*} \right) (\bar{\theta}_\alpha - \bar{w}_{,\alpha}) \right. \right. \\ &\quad \left. \left. - c_{\alpha\beta\gamma\delta}^M u_{0\alpha,\beta}^{(r)*} \bar{u}_{0\gamma,\delta} + \lambda^{(r)*} \rho \left\{ h(w^{(r)*} \bar{w} + u_{0x}^{(r)*} \bar{u}_{0x}) + I \theta_x^{(r)*} \bar{\theta}_x \right\} \right\} \right] n_{\partial A^i} \cdot \mathbf{V}^i dS, \end{aligned} \quad (41)$$

The optimality conditions of the Lagrangian function L with respect to $(u_0^{(r)*}, \bar{w}^{(r)*}, \theta^{(r)*})$, $(\bar{u}_0, \bar{w}, \bar{\theta})$ and A_λ are expressed as shown below:

$$\begin{aligned} a\left(\left(u_0^{(r)*}, w^{(r)*}, \theta^{(r)*}\right), (\bar{u}_0, \bar{w}, \bar{\theta})\right) \\ = \lambda^{(r)} b\left(\left(u_0^{(r)*}, w^{(r)*}, \theta^{(r)*}\right), (\bar{u}_0, \bar{w}, \bar{\theta})\right), \forall (\bar{u}_0, \bar{w}, \bar{\theta}) \in U, \end{aligned} \quad (42)$$

$$\begin{aligned} a\left(\left(u_0^{(r)*}, w^{(r)*}, \theta^{(r)*}\right), (\bar{u}_0, \bar{w}, \bar{\theta})\right) \\ = \lambda^{(r)} b\left(\left(u_0^{(r)*}, w^{(r)*}, \theta^{(r)*}\right), (\bar{u}_0, \bar{w}, \bar{\theta})\right), \forall (u_0^{(r)*}, w^{(r)*}, \theta^{(r)*}) \in U, \end{aligned} \quad (43)$$

$$b\left(\left(u_0^{(r)*}, w^{(r)*}, \theta^{(r)*}\right), (\bar{u}_0, \bar{w}, \bar{\theta})\right) = A_\lambda, \quad (44)$$

$$\dot{A}_\lambda (\lambda^{(r)} - \hat{\lambda}^{(r)}) = 0, \quad (45)$$

$$A_\lambda \geq 0. \quad (46)$$

Using the same procedure as in the case of the eigenvalue maximization problem, the shape gradient function of this problem is derived as shown in Eq. (47) by considering the relationship in Eq. (48).

$$\begin{aligned} G_{\partial A^i} = 1 - A_\lambda \left\{ -c_{\alpha\beta\gamma\delta}^B \theta_{(\alpha,\beta)}^{(r)*} \bar{\theta}_{(\gamma,\delta)} - k c_{\alpha\beta}^S \left(\theta_\beta^{(r)*} - w_{,\beta}^{(r)*} \right) (\bar{\theta}_\alpha - \bar{w}_{,\alpha}) \right. \\ \left. - c_{\alpha\beta\gamma\delta}^M u_{0\alpha,\beta}^{(r)*} \bar{u}_{0\gamma,\delta} + \lambda^{(r)*} \rho \left\{ h(w^{(r)*} \bar{w} + u_{0x}^{(r)*} \bar{u}_{0x}) + I \theta_x^{(r)*} \bar{\theta}_x \right\} \right\}, \end{aligned} \quad (47)$$

$$(\bar{u}_0, \bar{w}, \bar{\theta}) = \frac{A_\lambda \left(u_0^{(r)*}, w^{(r)*}, \theta^{(r)*} \right)}{b\left(\left(u_0^{(r)*}, w^{(r)*}, \theta^{(r)*}\right), \left(u_0^{(r)*}, w^{(r)*}, \theta^{(r)*}\right)\right)}. \quad (48)$$

4. Shape optimization method for determining the optimal free boundaries of stiffened shells

4.1. Modified H^1 gradient method for shells

The non-parametric shape optimization method described here for the design of the stiffened thin-walled structures is based on the H^1 gradient method, which is also called the traction method and is a type of gradient method in a Hilbert space. The original traction method was proposed by Azegami in 1994 [28,29]. The authors have modified the original traction method for shell optimization [30–32], and developed it to deal with the shape optimum design of stiffeners on thin-walled structures [18]. It is a node-based shape optimization method that can treat all nodes as design variables and does not require any shape design parametrization. This approach makes it possible to obtain the optimal boundary shapes of stiffened shell structures. As shown in Fig. 4, the Dirichlet conditions are defined for a pseudo-elastic shell in the case of boundary shape optimization of stiffeners and the basic structure with this method. A distributed force proportional to the shape gradient function $-G_{\partial A^i}$ is applied in the tangential direction to surfaces of the basic structure and stiffeners. The analysis for shape variation is called the velocity analysis. The shape gradient function is not applied directly to the shape variation but rather is replaced by a force, which varies shapes of stiffeners and the basic structure. This makes it possible both to reduce the objective functional and to maintain the smoothness, i.e., mesh regularity, which is the most distinctive feature of this method.

Considering the design velocity $\mathbf{V}^i = \{V_n^i\}_{n=1,2,3}$ as a combination of the in-plane velocity $\{\mathbf{V}_{0x}^i\}_{x=1,2}$ and the out-of-plane velocity

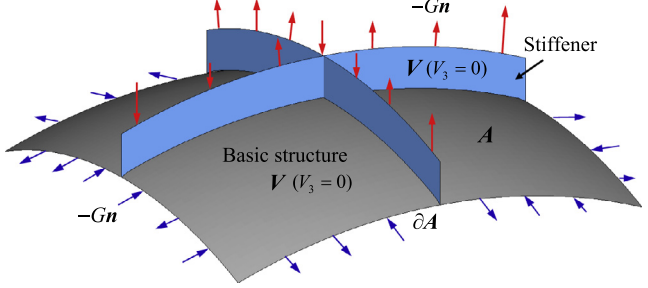


Fig. 4. Schematic of the parameter-free optimization method.

ity V_3^i , the governing equation of the velocity analysis for $\mathbf{V}^i = (V_{0x}^i, V_{0y}^i, V_3^i)$ is expressed as Eq. (49). To obtain the optimal free boundary shapes, an additional constraint is put on the variation in the normal direction to surfaces of the basic structure and stiffeners (i.e., $V_3^i = 0$) as shown in Fig. 4, as it is assumed that the stiffened thin-walled structure do not vary in their out-of-plane directions.

$$\begin{aligned} a\left(\left(\mathbf{V}_{0x}^i, V_3^i, \theta\right), (\bar{u}_0, \bar{w}, \bar{\theta})\right) \\ = -\langle Gn, (\bar{u}_0, \bar{w}, \bar{\theta}) \rangle, (\mathbf{V}_{0x}^i, V_3^i, \theta) \in C_\Theta, \forall (\bar{u}_0, \bar{w}, \bar{\theta}) \in C_\Theta, \end{aligned} \quad (49)$$

where C_Θ is expressed as

$$C_\Theta = \left\{ \left(V_{0_1}^i, V_{0_2}^i, V_3^i, \theta_1, \theta_2 \right) \in (H^1(A))^5 \mid \text{satisfy the constraints of shape variation on } \partial A \text{ and } V_3^i = 0 \text{ on } A \right\}. \quad (50)$$

Here we can confirm that the domain variation \mathbf{V}^i determined by the velocity analysis reduces the Lagrangian functional L . When the eigenvalue equation, the adjoint equation and the constraints are satisfied, the perturbation expansion of the Lagrangian functional L can be written as

$$\Delta L = \left\langle Gn, s \Delta \mathbf{V}^i \right\rangle + O(|\Delta s|^2). \quad (51)$$

Substituting Eq. (49) into Eq. (31) and taking into account the positive definitiveness of $a((u_0^{(r)}, w^{(r)}, \theta^{(r)}), (u_0^{(r)}, w^{(r)}, \theta^{(r)}))$, based on the positive definitiveness of the elastic tensors $c_{\alpha\beta\gamma\delta}^B$, $c_{\alpha\beta}^S$ and $c_{\alpha\beta\gamma\delta}^M$,

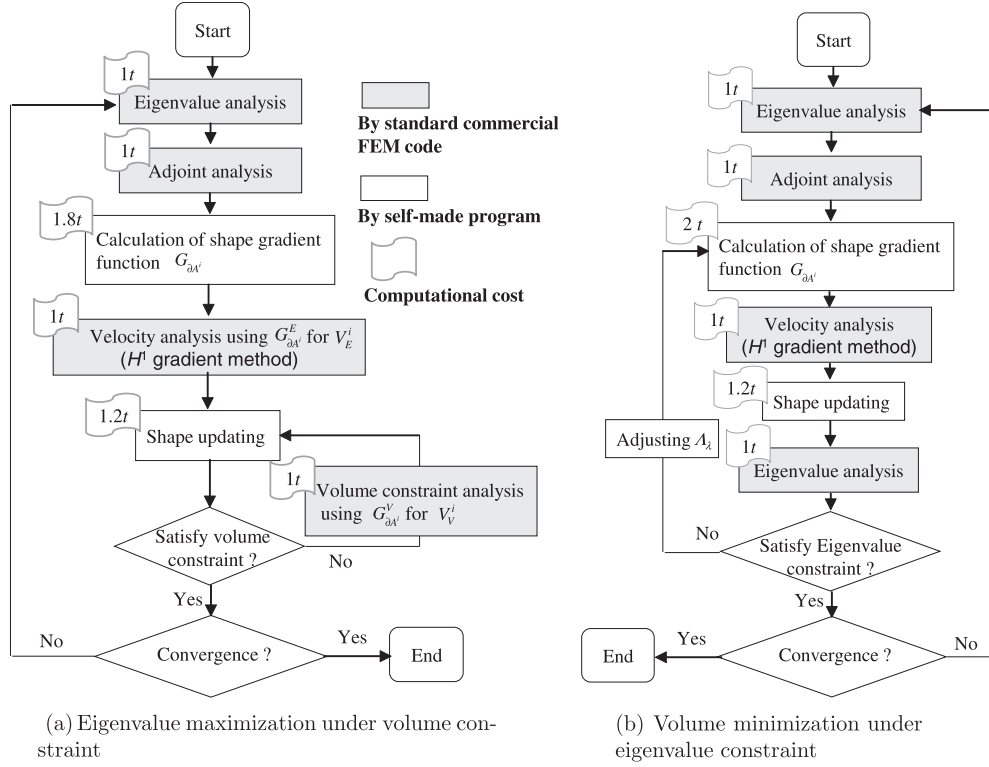
$$\exists \alpha > 0 : a(\xi, \xi) \geq \alpha \|\xi\|^2, \forall \xi \in U, \quad (52)$$

the following relationship is obtained when Δs is sufficiently small:

$$\Delta L = -a(\Delta s \mathbf{V}^i, \Delta s \mathbf{V}^i) < 0. \quad (53)$$

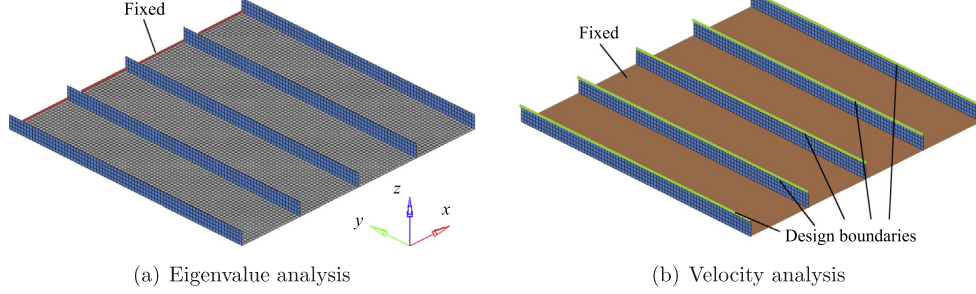
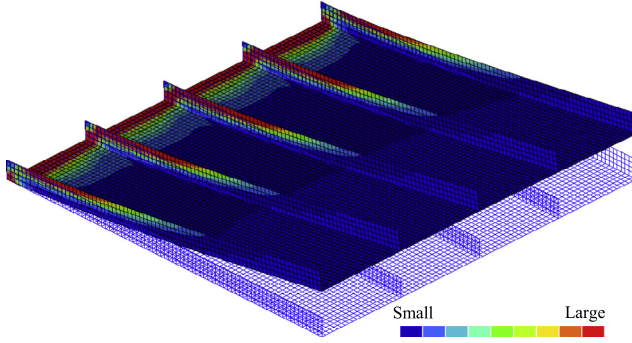
In problems where convexity is assured, this relationship definitely reduces the Lagrangian functional in the process of changing the domain using the design velocity field \mathbf{V}^i determined by Eq. (49).

For the regularity of the shape optimization problems, it was theoretically discussed in a previous paper of Azegami et al. [29] by using the regularity theorem for elliptic boundary value problems [33,34]. It is confirmed that a design domain reshaped by the domain variation \mathbf{V}^i obtained in Eq. (49) has a boundary that agrees with the original smoothness on ∂A^i , and has a smoother boundary for one-time differentiability than that obtained by the direct gradient method in which the boundary is moved in proportion to the shape gradient. Therefore, in the case of initial strict smoothness, the boundary smoothness can be maintained in the iterations by our proposed method. It suggests that the stiffness tensor in the governing Eq. (49) serves as a smoother for maintaining mesh regularity.



(a) Eigenvalue maximization under volume constraint

(b) Volume minimization under eigenvalue constraint

Fig. 5. Schematic of the non-parametric shape optimization method for natural vibration design of stiffened shells.**Fig. 6.** Boundary conditions of design Example 1.**Fig. 7.** The 1st natural mode.

4.2. Volume constraint

Here, we describe the approach for satisfying the volume constraint defined in Eq. (15). In the proposing gradient method, $G_{\partial A^i} n$ is used as a distributed sensitivity force aforementioned. Let's

consider to decompose the shape gradient density function $G_{\partial A^i}$ to $G_{\partial A^i}^E$ and $G_{\partial A^i}^V$ as shown in Eqs. (54)–(56).

$$G_{\partial A^i} = G_{\partial A^i}^E + G_{\partial A^i}^V, \quad (54)$$

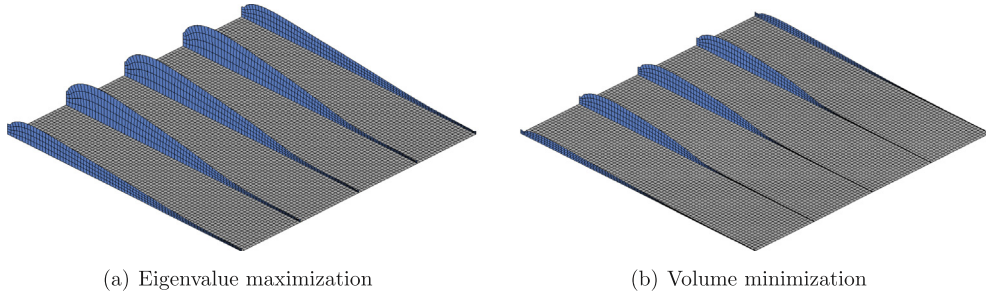
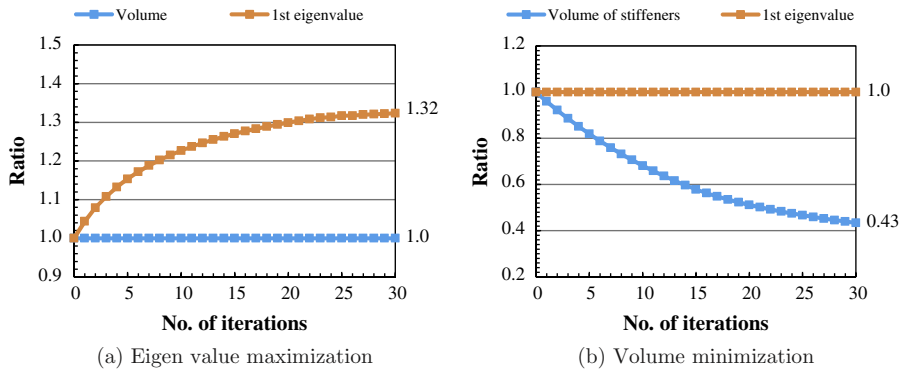
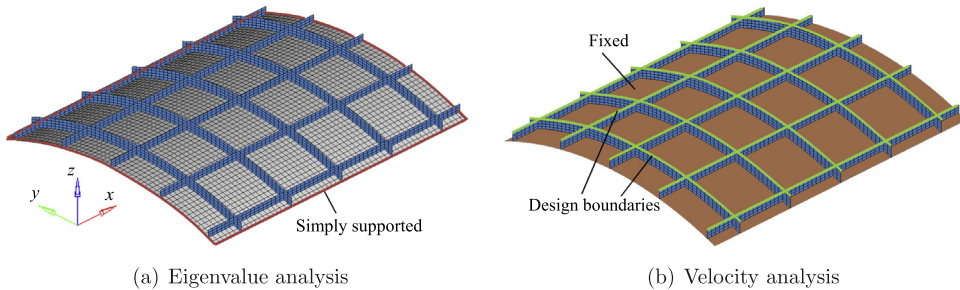
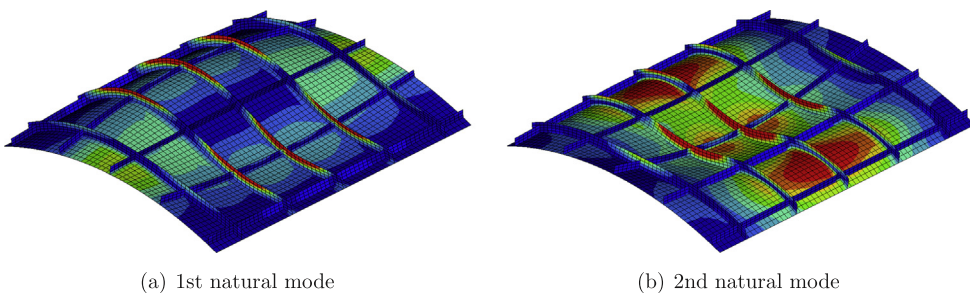
$$\begin{aligned} G_{\partial A^i}^E &= -c_{\alpha\beta\gamma\delta}^B \theta_{(\alpha,\beta)}^{(r)*} \bar{\theta}_{(\gamma,\delta)} - k c_{\alpha\beta}^S \left(\theta_{\beta}^{(r)*} - w_{,\beta}^{(r)*} \right) \left(\bar{\theta}_{\alpha} - \bar{w}_{,\alpha} \right) \\ &- c_{\alpha\beta\gamma\delta}^M u_{0\alpha,\beta}^{(r)*} \bar{u}_{0\gamma,\delta} + \lambda^{(r)} \rho \left\{ h \left(w^{(r)*} \bar{w} + u_{0\alpha}^{(r)*} \bar{u}_{0\alpha} \right) + I \theta_{\alpha}^{(r)*} \bar{\theta}_{\alpha} \right\}, \end{aligned} \quad (55)$$

$$G_{\partial A^i}^V = A_M. \quad (56)$$

The distributed sensitivity forces $G_{\partial A^i}^E n$ and $G_{\partial A^i}^V n$ can be independently applied to the fictitious elastic stiffener or basic shell to obtain \mathbf{V}_E^i and \mathbf{V}_V^i . It is possible to satisfy the volume constraint by adjusting the magnitude of the Lagrange multiplier A_M , or $G_{\partial A^i}^E n$. A_M is determined by the repeated calculation per iteration since the relation of the shell volume and A_M is not linear. The stiffener or the basic shell shape X^i is updated by $\mathbf{X}^i (= \mathbf{V}_E^i + \mathbf{V}_V^i)$.

$$\mathbf{X}^i = \mathbf{X}^{refi} + \mathbf{V}_E^i + \mathbf{V}_V^i, \quad (57)$$

where \mathbf{X}^{refi} denotes the referenced shape, or the shape at the previous iteration.

**Fig. 8.** Optimization results of design Example 1.**Fig. 9.** Iteration histories of design Example 1.**Fig. 10.** Boundary conditions of design Example 2.**Fig. 11.** Natural modes of design Example 2.

4.3. Flowchart of the shape optimization system

Flowcharts of the shape optimization systems developed for the design problems of the eigenvalue maximization and the volume minimization are schematized in Fig. 5(a) and (b), respectively. It shows that overall procedures for the two design problems are similar except for the constraint analysis. Firstly, the eigenvalue

analysis (Eq. (7)) is done using a standard commercial FEM code, in which the element quality of the model is inspected in order to guarantee the mesh regularity. For quasi self-adjoint relationships expressed in Eqs. (33) and (48), the adjoint analysis is not necessary in this study. Then, outputs of the analyses are utilized to calculate the shape gradient functions (Eqs. (32) and (47)). After that, the velocity analysis (Eq. (49)) is implemented, where a

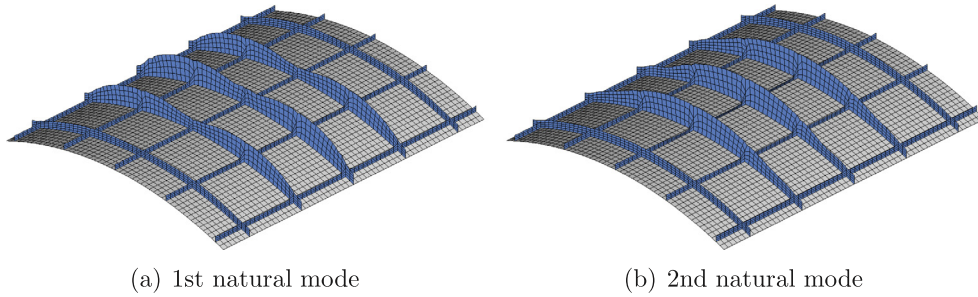


Fig. 12. Eigenvalue maximization results of design Example 2.

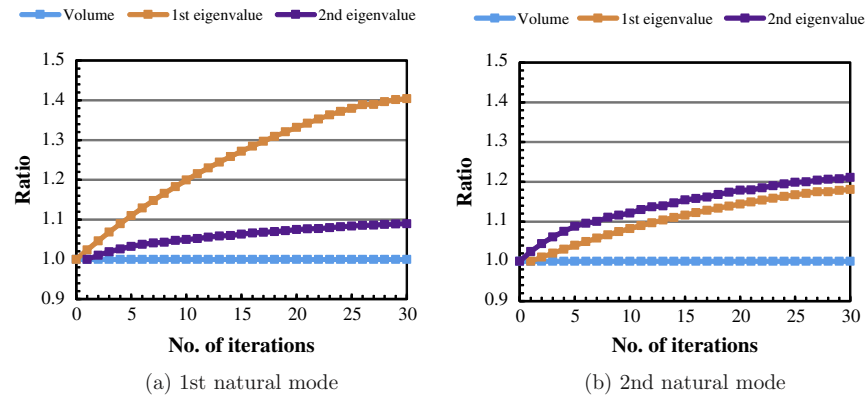


Fig. 13. Iteration histories of eigenvalue maximization.

distributed force proportional to the negative shape gradient function $-G_{\partial A^i}$ is applied to determine the design velocity field \mathbf{V}^i . Finally the shape is updated iteratively using the design velocity field \mathbf{V}^i . This process is repeated until the repeat count reaches the prescribed value and the changing rate of the objective function is lower than a threshold value. The main difference between the two procedures shown in Fig. 5(a) and (b) exists in the constraint satisfaction processes. In the volume-constrained eigenvalue maximization problem, as mentioned in Section 4.2, two velocity analyses are independently implemented for V_E^i and V_V^i to determine A_M by the repeated calculation in each iteration. On the other hand, in the eigenvalue-constrained volume minimization problem, one velocity analysis is carried out to obtain the composite shape variation \mathbf{V}^i and the constraint is satisfied by adjusting A_i repeatedly in each loop. Moreover, the computational cost of each main step in the two optimization procedures is shown in Fig. 5, using an eigenvalue analysis cost as the time reference unit t .

The advantages of the proposing method are summarized as follows:

- Complex free-boundary optimization problems with differently shaped stiffeners are easily solved, and the shapes of the stiffeners and the basic structures are simultaneously determined;
 - No shape parametrization in advance is needed, and therefore the obtained shapes are not influenced by the parametrization process;
 - As mesh smoothing is implemented simultaneously with shape updating, smooth and natural boundaries can be obtained without the jagged shape problem;
 - It can be implemented in combination with a commercial FEM code and the large-scale design variables problem of practical stiffened shells can be easily solved without high computational cost.

5. Results of numerical analysis

The proposed method was applied to four fundamental design problems in order to confirm its validity and practical utility for the stiffened thin-walled structures. In each design problem, the layout of stiffeners and the plate thickness are assumed to be

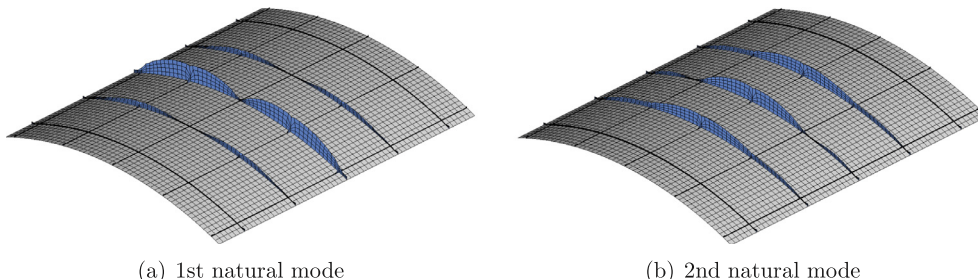


Fig. 14. Volume minimization results of design Example 2.

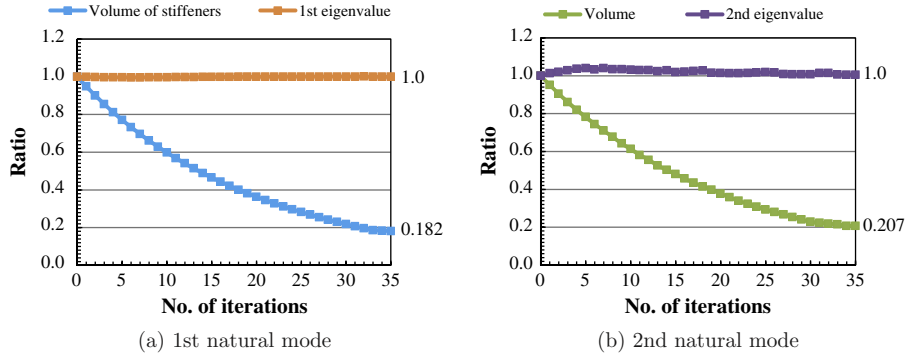


Fig. 15. Iteration histories of volume minimization.

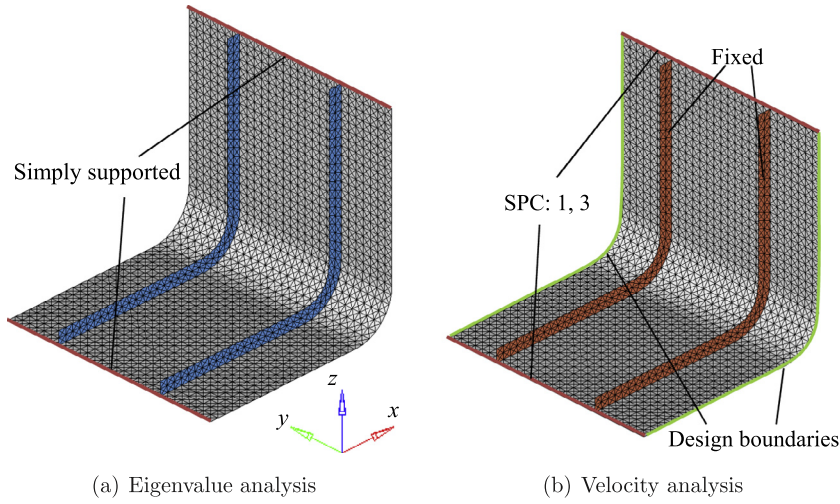


Fig. 16. Boundary conditions of design Example 3.

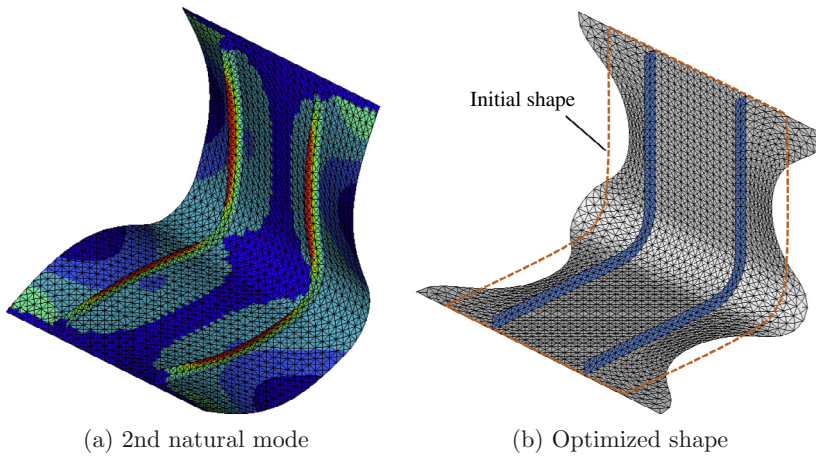


Fig. 17. Natural mode and optimization result of design Example 3.

constant during the optimization process. Moreover, the specified vibration mode is assumed to be the one which received the most attention in the practical design and is tracked by the approach described in Section 3.2.

5.1. Stiffened square plate design problem (Design Example 1)

The first design example considered is a cantilever square plate, which is stiffened by five parallel stiffeners with uniform initial height and equal intervals. Two kinds of optimum design problems

were solved by the proposed method. One is the 1st eigenvalue maximization problem subject to the constant volume constraint, and the other is its reciprocal volume minimization problem subject to the 1st eigenvalue constraint. Moreover, in each calculation, the 1st natural mode of the initial shape was tracked. The initial shape of the stiffened square plate is shown in Fig. 6(a) along with the boundary conditions of the eigenvalue analysis. The constraint conditions for the velocity analysis are shown in Fig. 6(b). One edge of the basic structure was fixed completely in the eigenvalue analysis, and the basic structure was fixed in the velocity analysis. The

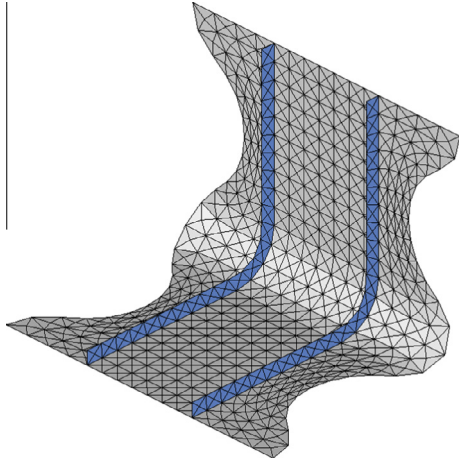


Fig. 18. Optimized shape with coarse mesh.

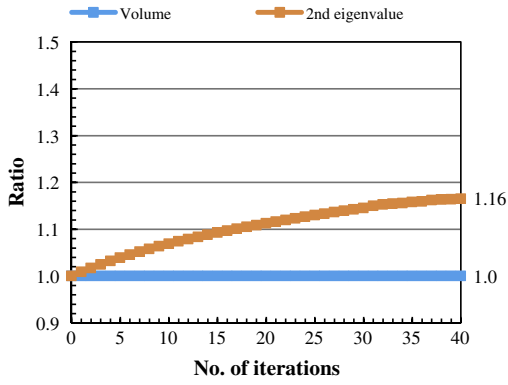


Fig. 19. Iteration histories of design Example 3.

longitudinal free boundaries of the stiffeners were treated as design boundaries.

Fig. 7 shows the 1st natural mode of the initial shape along with the distribution of the shape gradient function calculated by Eq. (32). The optimal stiffener boundaries obtained in each optimization problem are shown in Fig. 8(a) and (b), where the height of stiffeners around the free side of the square plate was reduced substantially, and stiffeners around the fixed side raised according to the magnitude of the shape gradient function. Though the sizes of the compressed elements are close to or smaller than their thickness, the accuracy of the finite element analysis is not influenced appreciably by using shell elements due to the low load resistance in these elements.

Iteration histories of the 1st eigenvalue and the volume for both problems are shown in Fig. 9(a) and (b), in which the values have been normalized to those of the initial shape. The results confirm that the 1st eigenvalue of the optimal shape was approximately 132% of that of the initial shape in the eigenvalue maximization problem, and that the optimal stiffener shapes obtained in the volume minimization problem were approximately 57% lighter in weight.

5.2. Stiffened roof shell design problem (Design Example 2)

The second design example is a stiffener shape optimization of a roof shell stiffened by latticed stiffeners. Both eigenvalue maximization and volume minimization were carried out by the proposed method. The initial shape is shown in Fig. 10(a) along with the boundary conditions of the eigenvalue analysis, where both the curved boundaries and the straight boundaries were simply supported. The constraint conditions for the velocity analysis are shown in Fig. 10(b), where the basic structure was fixed. The 1st and 2nd natural modes of the initial shape obtained by the eigenvalue analysis are shown in Fig. 11(a) and (b), respectively.

The specified 1st and 2nd eigenvalues were maximized separately subject to the constant volume constraint, and each of the natural modes was tracked. The optimal stiffener boundaries obtained in each eigenvalue maximization problem are shown in Fig. 12. According to the magnitude of the shape gradient function, the five stiffeners along the straight boundary of the basic structure were reduced, and the reduced volume shifted to the central stiffeners along the curved boundary of the basic structure. Iteration histories of the compliance and the volume for both problems are shown in Fig. 13(a) and (b), in which the values have been normalized to those of the initial shape. Compared with the initial shape, the 1st and the 2nd eigenvalues increased approximately 40% and 9% respectively in the 1st eigenvalue maximization, and increased approximately 18% and 21% respectively in the 2nd eigenvalue maximization. The results show that the raised stiffeners along the curved boundary contribute to increase both the 1st eigenvalue and the 2nd eigenvalue, and also show that the different optimum shapes obtained in the two eigenvalue maximization problems result in various increasing rates of the 1st and the 2nd eigenvalues.

In the case the 1st and the 2nd eigenvalues or other eigenvalues cannot be maximized separately, but be considered synthetically for practical reasons, the proposed method can be easily extended to a multi-objective optimization problem. The authors have recently proposed a multi-objective free-form optimization method for designing shell structures under multi-boundary conditions [35], and the multi-objective eigenvalue design problem can be solved similarly.

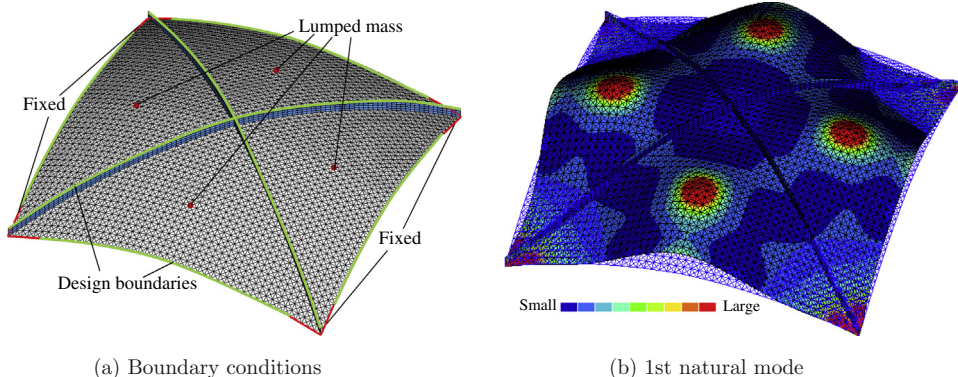


Fig. 20. Stiffened dome-shaped shell.

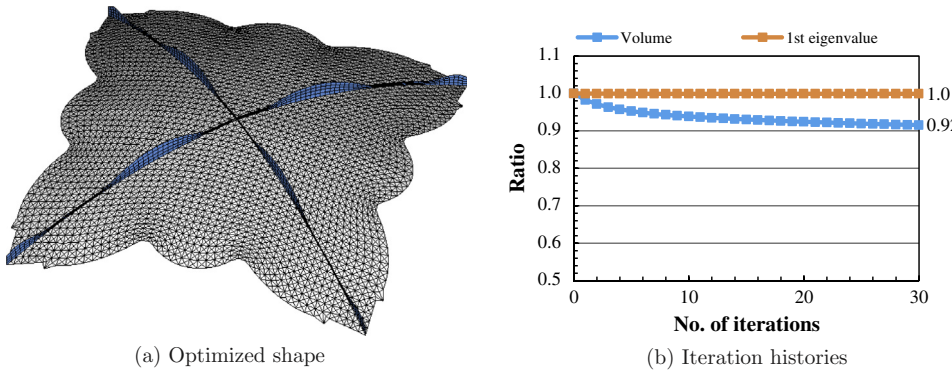


Fig. 21. Optimization results of design Example 4.

Furthermore, the 1st and 2nd eigenvalues were set as the constraint separately and the volume was minimized while tracking each of the natural modes. Fig. 14 shows the optimal stiffener shapes obtained in the volume minimization problem. Fig. 15(a) and (b) shows iteration histories of the compliance and the volume for the 1st and 2nd eigenvalues constraints, respectively. The volume of stiffeners shape decreased to 18.2% of the initial shape for the 1st eigenvalue constraint, and 20.7% of the initial shape for the 2nd eigenvalue constraint.

5.3. Stiffened L-shaped bracket design problem (Design Example 3)

A stiffened L-shaped bracket, like that shown in Fig. 16, was optimized as an example of the basic structure design problem. Two parallel stiffeners with uniform initial height were added at equal intervals on the surface of the bracket. Design boundaries were set at the left and the right sides of the basic structure. Fig. 16(a) shows the boundary conditions in the eigenvalue analysis, in which the lower and the upper edges were simply supported. In the velocity analysis as shown in Fig. 16(b), in addition to the constraints for maintaining the initial curvature, the stiffeners were fixed and x, z translational degrees of freedom of the lower and the upper edges were constrained. Fig. 17(a) shows the 2nd natural mode of the initial shape, where the color represents the distribution of the shape gradient function.

The 2nd vibration eigenvalue was maximized while tracking its natural mode and the initial volume was given as the constraint value. Fig. 17(b) shows the obtained shape. It is observed that smooth free-boundary shapes were obtained while maintaining the initial curvature, and that the higher sensitive portions near the constrained edges and the curved area were expanded and the lower sensitive portions were compressed. In order to investigate the influence of mesh size, the same L-shaped bracket with coarse mesh was optimized, and the obtained form is shown in Fig. 18. The result shows that almost the same shape was obtained in spite of the different mesh size.

Fig. 19 shows the iteration convergence histories of the 2nd eigenvalue and the volume, where the values have been normalized to those of the initial form. The 2nd eigenvalue was increased by 16% while satisfying the constant volume constraint.

5.4. Stiffened dome-shaped shell design problem (Design Example 4)

The last design example is a stiffened dome-shape shell in which free boundaries of both stiffeners and the basic structure were treated as design boundaries. As shown in Fig. 20(a), four non-structural lumped masses were added symmetrically on the basic structure and the four corners were fixed completely in the eigenvalue analysis as well as in the velocity analysis. The

volume was minimized while tracking the 1st natural mode of the initial shape as shown in Fig. 20(b), and the 1st eigenvalue was given as an constraint value. Fig. 21(a) shows the optimized shape, in which smooth free-boundary shapes of both stiffeners and the basic structure were obtained according to the distribution of the shape gradient function in Fig. 20(b). Fig. 21(b) shows the iteration convergence of the 1st eigenvalue and the volume, where the values have been normalized to those of the initial form. The structure including stiffeners and the basic structure was approximately 8% lighter in weight while satisfying the constant eigenvalue constraint.

6. Conclusions

This paper has proposed a parameter-free shape optimization method for designing the shapes of stiffened thin-walled or shell structures in the natural vibration problem. The optimal free boundary shapes of either stiffeners or basic structures can be obtained with the proposed method. A specified eigenvalue maximization problem subject to a volume constraint can be solved along with its reciprocal problem in which volume reduction is the objective. The proposed method has been applied to typical design problems of stiffened thin-walled structures, and the numerical results showed that smooth optimal boundary shapes were obtained in each design problem to achieve the maximum eigenvalue or a lightweight structure. It has been demonstrated that the proposed method is an effective tool for designing optimal stiffeners as well as basic structures on thin-walled or shell structures.

Acknowledgement

This research was supported by grants-in-aid from the Yazaki Memorial Foundation for Science and Technology in Japan.

References

- [1] Alejandro RD, Kikuchi N. Solutions to shape and topology eigenvalue optimization problems using a homogenization method. *Int J Numer Meth Eng* 1992;35:1487–502.
- [2] Ma ZD, Kikuchi N, Cheng HC. Topological design for vibrating structures. *Comput Methods Appl Mech Eng* 1995;121:259–80.
- [3] Zhao C, Steven G, Xie Y. Evolutionary natural frequency optimization of thin plate bending vibration problems. *Struct Optim* 1996;11(3–4):244–51.
- [4] Cheng KT, Olhoff N. An investigation concerning optimal design of solid elastic plates. *Int J Solids Struct* 1981;17:305–23.
- [5] Luo J, Gea HC. A systematic topology optimization approach for optimal stiffener design. *Struct Optim* 1998;16:280–8.
- [6] Luo J, Gea HC. Optimal stiffener design for interior sound reduction using a topology optimization based approach. *ASME J Vib Acoust* 2003;125(3):267–73.
- [7] Liu Z, Hansen J, Oguamanam D. Eigenvalue sensitivity analysis of stiffened plates with respect to the location of stiffeners. *Struct Optim* 1998;16:155–61.

- [8] Ding X, Yamazaki K. Stiffener layout design for plate structures by growing and branching tree model (application to vibration-proof design). *Struct Multidiscip Optim* 2004;26:99–110.
- [9] Bojczuk D, Szeleblak W. Optimization of layout and shape of stiffeners in 2d structures. *Comput Struct* 2008;86:1436–46.
- [10] Chen B, Liu G, Kang J, Li Y. Design optimization of stiffened storage tank for spacecraft. *Struct Multidiscip Optim* 2008;36:83–92.
- [11] Cheng B, Xiao R, Zhao J, Cheng J. Optimal stiffener design of moderately thick plates under uniaxial and biaxial compression. *J Constr Steel Res* 2010;66(10):1218–31.
- [12] Herencia JE, Weaver PM, Friswell MI. Optimization of long anisotropic laminated fiber composite panels with t-shaped stiffeners. *AIAA J* 2007;45(10):2497–509.
- [13] Liu W, Butler R, Kim HA. Optimization of composite stiffened panels subject to compression and lateral pressure using a bi-level approach. *Struct Multidiscip Optim* 2008;36(3):235–45.
- [14] Virág Z. Optimum design of stiffened plates for different loads and shapes of ribs. *J Comput Appl Mech* 2004;5:165–79.
- [15] Patnaik SN, Sankaran GV. Optimum design of stiffened cylindrical panels with constraint on the frequency in the presence of initial stresses. *Int J Numer Meth Eng* 1976;10(2):283–99.
- [16] Yamazaki K, Aoki A. Optimal stiffener shape of thin plate structure against buckling. *Trans Jpn Soc Mech Eng Part A* 1991;57:412–6 [in Japanese].
- [17] Yamazaki K, Nagai H. Minimum compliance design technique of stiffener height of stiffened thin plate structure. *Trans Jpn Soc Mech Eng Part A* 1988;54:1430–3 [in Japanese].
- [18] Liu Y, Shimoda M. Parameter-free optimum design method of stiffeners on thin-walled structures. *Struct Multidiscip Optim* 2014;49:39–47.
- [19] Braibant V, Fleury C. Shape optimal design using b-splines. *Comput Methods Appl Mech Eng* 1984;44:247–67.
- [20] Bletzinger KU. A consistent frame for sensitivity filtering and the vertex assigned morphing of optimal shape. *Struct Multidiscip Optim* 2014;49:873–95.
- [21] Eldred MS, Venkaya VB, Anderson WJ. Mode tracking issues in structural optimization. *AIAA J* 1995;33(10):1926–33.
- [22] Allemand R. The modal assurance criterion-twenty years of use and abuse. *Sound Vib* 2003;37:14–21.
- [23] MacNeal RH. Finite elements: their design and performance. New York: Marcel Dekker, Inc.; 1994.
- [24] Hughes TJR. The finite element method-linear static and dynamic finite element analysis. Prentice-Hall; 1987.
- [25] Reissner E. The effect of transverse shear deformation on the bending of elastic plates. *J Appl Mech* 1945;67: A-69–A-77.
- [26] Haug EJ, Choi KK, Komkov V. Design sensitivity analysis of structural systems. Academic Press, INC; 1986.
- [27] Choi KK, Kim NH. Structural sensitivity analysis and optimization. New York: Springer; 2005.
- [28] Azeogami H. A solution to domain optimization problems. *Trans Jpn Soc Mech Eng Ser A* 1994;60:1479–86.
- [29] Azeogami H, Kaizu S, Shimoda M, Katamine E. Irregularity of shape optimization problems and an improvement technique. *Comput Aided Optim Des Struct* 1997;V:309–26.
- [30] Shimoda M, Tsuji J. Non-parametric shape optimization method for rigidity design of automotive sheet metal structures. *SAE, J Passenger Cars – Mech Syst* 2007;2006-01-0584:483–92.
- [31] Shimoda M, Iwasa K, Azeogami H. A shape optimization method for the optimal free-form design of shell structures. In: Proceedings of 8th world congress on structural and multidisciplinary optimization; 2009.
- [32] Liu Y, Shimoda M. Two-step shape optimization methodology for designing free-form shells. In: Inverse problems in science and engineering; 2013. Published online: 29 April 2013.
- [33] Pironneau O. Optimal shape design for elliptic systems. New York: Springer; 1984.
- [34] Ladyzhenskaya OA, Ural'tseva NN. Linear and quasilinear elliptic equations. New York: Academic Press; 1968.
- [35] Shimoda, M, Liu, Y, Yonekura, M. Multi-objective free-form optimization of shell structures. In: 53rd AIAA/ASME/ASCE/AHS/ASC structures, structural dynamics and materials conference. AIAA 2012-1755; 2012.